Petroleum Science 21 (2024) 2830–2838

Contents lists available at ScienceDirect

Petroleum Science

journal homepage: www.keaipublishing.com/en/journals/petroleum-science

Original Paper

Acoustic characterization of hydrate formation and decomposition in clay-bearing sediments

Yi-Jian Zhu [1], Xiao-Mei Yang [1], Xing Huang, Hao Li, Xiao-Hui Wang, Yi-Fei Sun, Peng Xiao, Chang-Yu Sun [*], Guang-Jin Chen [**]

State Key Laboratory of Heavy Oil Processing, College of Chemical Engineering and Environment, China University of Petroleum, Beijing, 102249, China

ARTICLE INFO

Article history:
Received 20 January 2024
Received in revised form
7 June 2024
Accepted 12 June 2024
Available online 13 June 2024

Edited by Min Li

Keywords:
Gas hydrate
Bentonite
Illite
P-wave velocity
Amplitude

ABSTRACT

Understanding the acoustic characteristics of hydrates in various sediments is crucial for hydrate resource detection and safe and efficient exploitation, as hydrate occurrence patterns vary greatly in different sediments. In this work, sediments with different bentonite contents, water saturations, and types were prepared to investigate the characteristics of P-wave velocity (reflecting the magnitude of hydrate saturation in the sediment) and amplitude (reflecting the degree of hydrate-sediment cementation) during hydrate formation and depressurization. During hydrate formation, the P-wave velocity and amplitude have similar trends. As clay content increases, the P-wave velocity increase rates quickened. On the other hand, the increased rate of P-wave velocity slows down with the increase of water saturation in the clay-bearing sediments. Comparing various types of sediment shows that the water absorption and swelling of bentonite reduce the pore space, speeding up the cementation of the hydrate with the sediment and increasing P-wave velocity at a faster rate. Correspondence between P-wave velocity and hydrate saturation is strongly related to sediment type, clay content, and water saturation. The rapidly decreasing amplitude in the early stage of hydrate depressurization indicates that hydrate in clay-bearing sediments is weakly cemented to the sediments, which is prone to stratigraphic instability. The findings of this study offer guidance for hydrate resource assessments in clay-bearing sediments as well as geologic risk estimations during hydrate mining.

1. Introduction

Natural gas hydrate (NGH), an ice-like nonstoichiometric solid compound, is composed of water and gas molecules (mainly methane) under low temperature and high pressure (Chen et al., 2015; Sloan, 2003; Wang et al., 2019a). At present, NGH deposits with significant resources are found in the sea floor and permafrost regions (Zhang et al., 2023). Most hydrate resources in China are found in South China Sea seafloor sediments that are abundant with clay minerals such as montmorillonite, chlorite, illite, and kaolin (Zhao and Wan, 2014; Zhu et al., 2023). The gas production characterization of NGHs, the self-characterization of clay minerals, and the mechanical properties of reservoirs have been intensively studied in different clay-bearing sediments in the laboratory (Guo et al., 2020; Li et al., 2019; Lv et al., 2019; Shi et al., 2022; Wu et al., 2018; Yan et al., 2019). Numerous researches have clarified how clay minerals' water absorbing and swelling characteristics, their effects on water activity, and how their structure affects hydrate formation and decomposition (Kadoura et al., 2016; Wu et al., 2020). However, there are few reports of ultrasonic characteristics of hydrate formation or decomposition in clay-bearing sediments, as ultrasonic logging, density logging, resistivity logging, and Gamma-ray are commonly used for identifying resources.

The P-wave and S-wave are widely used as two important ultrasonic waves for the detection of hydrate resources (Ren et al., 2020b). The S-waves have a restricted application because they can only pass through solids. In addition, hydrate cannot be reliable detected independently by density logging, resistance logging, etc., according to the study of field logging data (Qian et al., 2018; Wang et al., 2018). Therefore, the detection of marine hydrate resources frequently made use of P-waves. The elastic modulus calculated

* Corresponding author.
** Corresponding author.
E-mail addresses: cysun@cup.edu.cn (C.-Y. Sun), gjchen@cup.edu.cn (G.-J. Chen).
[1] These authors contributed equally to this work.

https://doi.org/10.1016/j.petsci.2024.06.008

from the P-wave velocity (V_P) also reflected the stratum stiffness (Ren et al., 2020a). Numerous hydrate formation and decomposition studies had been carried out in the laboratory to better understand the acoustic characteristics of NGHs in sediments (Ding et al., 2020; Kim et al., 2013; Liu et al., 2019). The hydrate and sand sediments continued to cement with the hydrate saturation raised, and the wave velocity increased (Waite et al., 2009). In the sand unconsolidated sediment, the change in V_P and S-wave velocity (V_S) was not sensitive to the THF hydrate saturation below 40% (volume). It was inferred that THF hydrates first formed in the pore space and then grew outside of the pore space (Yun et al., 2005). In consolidated sediments, the V_P increased as THF hydrate saturation and confining pressure increased (Sadeq et al., 2018). Seismic wave velocity of CO_2 hydrate formation processes in fine-grained sediments under different vertical effective stresses was measured by Kim et al. (2013). The trend of hydrate saturation and V_S indicated that hydrate was weakly cemented to the clayey silt sediments when hydrate saturation was below 28% (volume), and the trend of V_P indicated that the effect of hydrate-sediment cementation was not significant at hydrate saturations below 47% (volume). Wang et al. (2019b) measured the variation pattern of acoustic properties during CH_4 hydrate formation in sandy and clay hydrate-bearing sediments. The results showed the seismic wave velocity in sandy sediments changed significantly with hydrate formation/decomposition, while it changed less in clay hydrate-bearing sediments. Micro-distribution patterns of different hydrate decomposition stage in South China Sea sediments were investigated by Bu et al. (2019) using acoustic features. The rapidly decreasing wave speeds indicated the hydrate was decomposing at contact with the sediment, and slowly decreasing wave speeds demonstrated the hydrate was suspended in the pores of the particles. Although the acoustic properties of hydrate formation and decomposition have been extensively studied in different sediments, the effect of specific reservoir characteristics on the acoustic properties has not been systematically investigated.

Drilling data from the South China Sea sites show that the main clay minerals in the sediments sampled at some stations are montmorillonite and illite (Ning et al., 2020). Hydrate reservoirs in the sea area were mainly dominated by weakly consolidated sediments that were not rock-forming and have poor mechanical strengths (Ye et al., 2020). For resource detection in hydrate reservoirs and evaluation of changes in reservoir stiffness strength, the acoustic properties of hydrate endowed in various characteristic sediments are essential. Accurate resource estimation and safe and effective hydrate exploitation depend on having a better understanding of the acoustic properties of various hydrate reservoir conditions. In this work, bentonite and illite were selected to be compounded with quartz sand to form the hydrate reservoirs. The acoustic characteristics of quartz sand, bentonite-sandy sediment, and illite-sandy sediment under different experimental conditions were investigated during CH_4 hydrate formation and depressurization mining. The obtained results are expected to offer guidance for hydrate resource assessments in clay-bearing sediments as well as geologic risk estimations during hydrate mining.

2. Experimental

2.1. Apparatus and materials

The schematic of experimental apparatus is shown in Fig. 1. The whole experimental system is divided into five parts, including gas injection system, reaction system, temperature control system, data acquisition system, and gas recovery system. The gas injection system consists of experimental gas and buffer tank. The major component of the reaction system is a 2 L (Φ130 × 150 mm) stainless steel reactor. The stainless steel ring inside the reactor is used to compact the sediments. Thus, the effective volume of the reactor is 1.485 L. The maximum adjustable distance between the upper and lower ultrasonic probes is 60 mm. The temperature sensor in the reactor has a measuring accuracy of ±0.01 K, and the pressure sensor has a measuring accuracy of 0.01 kPa. Temperature of air bath in the temperature control system can be adjusted between 263 and 303 K. The data acquisition system consists of two parts: temperature and pressure data acquisition, and acoustic data acquisition. The back pressure valve, gas-liquid separator, and the collection tank together form the gas recovery system.

CH_4 and N_2 of 99.99 % (mol) were supplied by Beijing Haipu gas company. Quartz sands (40–60 mesh), bentonite (800 mesh), and illite (800 mesh) used as the hydrate sediments were supplied by Hengyuan New Material Co. The deionized water was prepared in our laboratory.

2.2. Experimental procedures

The reactor, quartz sand, clay and deionized water were precooled at 273.15 K before the experiment. Then, they were combined well in proportion and immediately fed into a reactor, which minimized the migration of water so as to generate a more homogeneous hydrate reservoir. It is known that the degree of homogeneity of the hydrate has an enormous impact on the acoustic characteristics (Ren et al., 2020a). After the device tightness test with high-pressure N_2, CH_4 gas was injected into the reactor to generate a pressure of approximately 8 MPa. At this time, the phase equilibrium pressure of CH_4 hydrate calculated by Chen-Guo model (Chen and Guo, 1998; Wang et al., 2021) was 3.11 MPa, which made CH_4 hydrate form rapidly. When the pressure in the reactor no longer decreased, it marked the end of CH_4 hydrate formation. Excess CH_4 free gas in the reactor was vented until the reactor pressure dropped to around 0.5 MPa over the CH_4 hydrate phase equilibrium pressure. Once the temperature and pressure in the reactor stabilized again, depressurization was used to mine CH_4 hydrate. The back pressure valve 5 was adjusted to 2.0 MPa during CH_4 hydrate mining. After the temperature and pressure in the reactor had stabilized and pressure in the collection tank 2 no longer increased, the experimental process was considered to be finished.

3. Results and discussion

In this work, bentonite contents, water saturations, and sediments were investigated to study the acoustic properties of CH_4 hydrate formation and decomposition processes. The detailed experimental parameters are shown in Table 1. The amplitude and P-wave velocity were used to experimentally characterize the acoustic parameters in sediments containing clay.

3.1. CH_4 hydrate formation

3.1.1. Effect of bentonite content

The influence of 0%, 5%, 10%, 15% (mass) bentonite content in sandy sediments on the acoustic properties was investigated during CH_4 hydrate formation. The variation of pressure and hydrate saturation with time for different bentonite content are shown in Fig. 2(a) and (b), respectively. CH_4 hydrate forms rapidly when the CH_4 gas pressure in the 275.15 K reactor reaches about 8 MPa. In sediments with 0% (mass) and 15% (mass) bentonite content, the rates of pressure decrease and hydrate saturation increase are comparable, but they does not result from the same cause. In sediments with 0% (mass) bentonite content, there is sufficient free water and CH_4 gas to provide sufficient conditions for hydrate

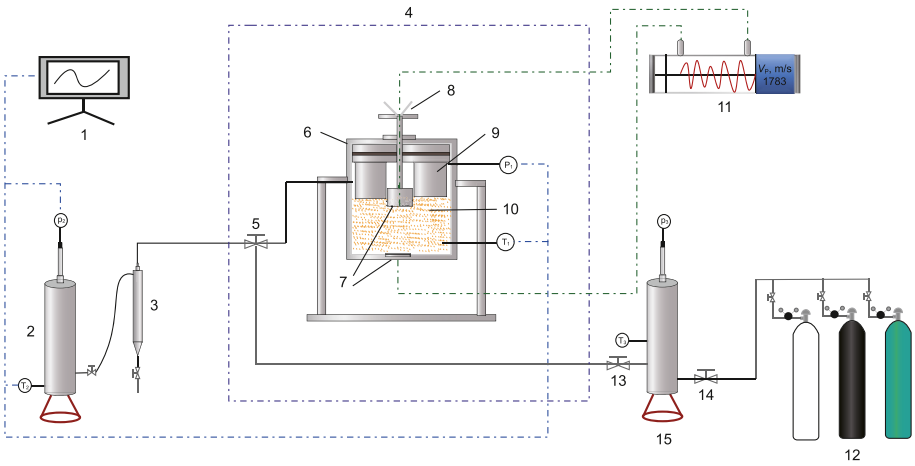

Fig. 1. Schematic of experimental apparatus: 1 temperature/pressure data acquisition system, 2 collection tank, 3 gas-water separator, 4 air bath, 5 back pressure valve, 6 reactor, 7 ultrasonic probe, 8 hand lever, 9 stainless steel ring, 10 sediment, 11 acoustic data acquisition system, 12 gas cylinder, 13, 14 valve, 15 buffer tank.

Table 1
Experimental parameters.

Runs	1	2	3	4	5	6	7
Sand:Clay, % (mass)	100:0	95:5	90:10	85:15	90:10	90:10	90:10
Clay type	\	bentonite	bentonite	bentonite	bentonite	bentonite	illite
Water saturation, % (volume)	30	30	30	30	40	50	30
Hydrate saturation, % (volume)	27.4	19.0	15.2	14.1	29.6	44.6	29.4
Mining pressure, MPa	2.0	2.0	2.0	2.0	2.0	2.0	2.0
Mining temperature, K	275.15	275.15	275.15	275.15	275.15	275.15	275.15
P-wave velocity, m/s[a]	2830	3088	2728	1532	2904	3116	3792

[a] The P-wave velocity here is the velocity at the end of hydrate formation before the free gas is vented.

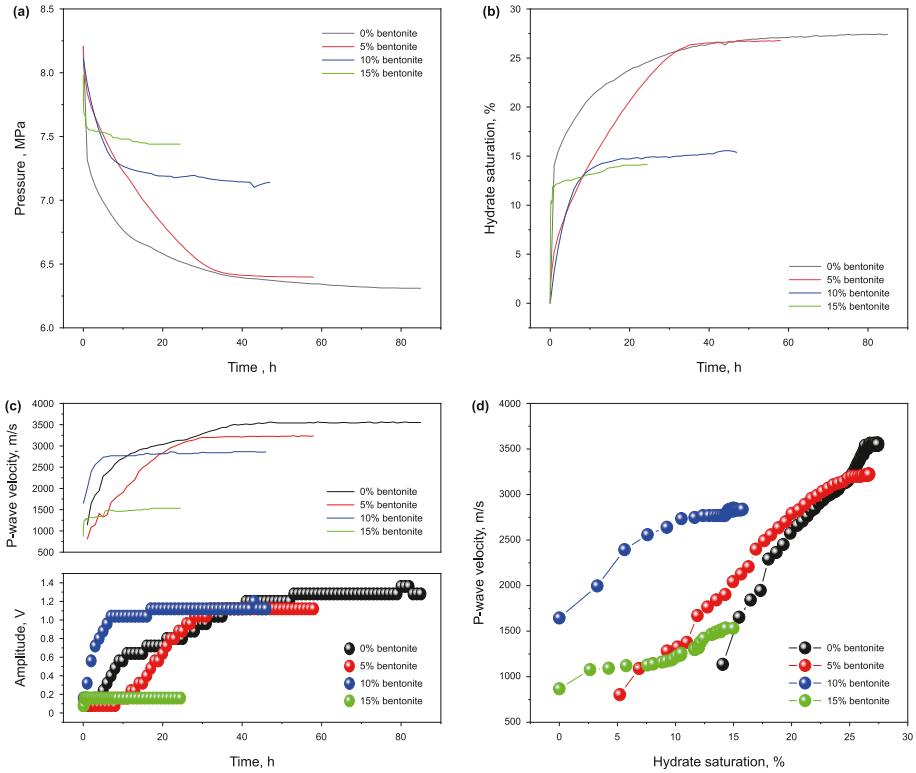

Fig. 2. Variation of **(a)** pressure; **(b)** hydrate saturation; **(c)** P-wave velocity and amplitude with time and **(d)** P-wave velocity with hydrate saturation in different bentonite content sediments.

formation, while in 15% (mass) bentonite containing sediments, only a small amount of free water is involved in hydrate formation due to the effect of bentonite water absorption. However, the addition of bentonite provides more nucleation sites for hydrate formation, which results in an initial hydrate formation rate similar to that in 0% (mass) bentonite containing sediments. In bentonite-containing sediments, the swelling of the bentonite as it absorbs water leads to a reduction in the amount of free water that can be used to form hydrates directly with CH_4, whereas capillary water and gravitational water can continue to form hydrates with CH_4 only when the water saturation is high (Zhang et al., 2022). This means that in bentonite-bearing sediments, free water first forms hydrates with CH_4, followed by capillary water and gravitational water then forms hydrates with CH_4. For this reason, compared to sediments containing 0% (mass) of bentonite, the hydrate formation rate in sediments containing 5% and 10% of bentonite is lower. Hydrate saturation is about 27% (volume) in the sediments with 0% (mass) and 5% (mass) bentonite content, while the hydrate saturation is 15% (volume) and 14% (volume) in the sediments with 10% (mass) and 15% (mass) bentonite content, respectively, because of less water available for the hydrate formation.

Fig. 2(c) illustrates the variation of P-wave velocity and amplitude with time. As hydrate continues to form, hydrate fills and cements the sediments, and P-wave velocity increases with hydrate saturation (Li et al., 2016; Ren et al., 2010). The hydrate saturation decreases with increasing clay content, and the P-wave velocity values of sediments with 0%, 5%, 10% and 15% (mass) bentonite content are 3551, 3226, 2855, and 1532 m/s, respectively. From Fig. 2(b) and (c), it can be seen that sediments with 0% (mass) and 5% (mass) bentonite content, sediments with 10% (mass) and 15% (mass) bentonite content, have approximately the same saturation but quite different P-wave velocity. This may be because hydrates first form on the surface of the bentonite particles and cement to each other with the bentonite particles as the bentonite content of the sediment increases. This causes a quick increase in amplitude in sediments with high bentonite content. Hydrates in sediments without bentonite first form in the pores and then gradually cement to the sediments as hydrate saturation increases, which results in a slower increase in amplitude. Different sediments have varying degrees of ultrasonic signal attenuation. As shown in Fig. 2(d), the hydrate saturation points at which the P-wave initially emerged varies amongst bentonite deposits with varying contents. Hydrate saturation is 14.1%, 5%, 0%, and 0% in 0%, 5%, 10%, and 15% bentonite content of the sediments, respectively, when the P-wave is first detected. That is, the attenuation of acoustic energy by the sediments diminishes as the bentonite content in the sediments rises. In Fig. 2(d), the hydrate saturation and P-wave velocity are approximately positively correlated linearly. As the bentonite content increases, the growth rate of P-wave velocity slows down with increasing hydrate saturation. This can be attributed to more hydrate cement with bentonite in the higher bentonite content sediments, which made the stiffness of the whole reservoir weak.

3.1.2. Effect of water saturation

As illustrated in Fig. 3(a) and (b), more water is involved in hydrate with the water saturation increased. The hydrate saturation of 30%, 40%, and 50% (volume) water saturation are 15.4%, 29.6%, and 44.6% (volume) respectively. In bentonite-containing sediments, elevated water saturation contributes to the formation of hydrates by utilizing more capillary and gravitational water.

As the water saturation rises, the rate of growth in P-wave velocity and amplitude decreases, as presented in Fig. 3(c). We speculate that this might be due to the fact that excess water slows down the mutual cementation between bentonite-hydrate-sand, while the enhancement of the overall stiffness of the reservoir depends on the cementation between hydrate and sand. P-wave velocity has similar rising rates with hydrate saturation at different water saturation, but large differences in P-wave velocity at the same hydrate saturation, as shown in Fig. 3(d). The P-wave velocity is 2817 m/s for the initial 30% (volume) water saturation, while the P-wave velocity is 2084 m/s for the initial 40% (volume) water saturation, and the P-wave velocity is only 1308 m/s for the initial 50% (volume) water saturation when hydrate saturation is about 15% (volume). This result implies that hydrate acts as a “binder” to rapidly bind bentonite particles to sand in low water-saturated bentonite-containing sediments. Besides, the P-wave velocity increases quickly in lower water-saturated sediments due to the fast cementing of deposits, which permits ultrasonic high-frequency energy to pass through. Hydrates may initially cement with bentonite or remain suspended independently in the pore when water saturation rises in bentonite containing sediments, which makes it difficult for high-frequency ultrasound energy to pass through the deposit. This results in much larger P-wave velocity and amplitudes in bentonite-bearing sediments with low water saturation than in those with high water saturation at the same hydrate saturation.

3.1.3. Effect of sediments

The different rates of pressure reduction indicate that the hydrate formation rate in quartz sand is faster than that in clay-bearing sediments, as shown in Fig. 4(a). This can be attributed to the fact that pure quartz sand has large pores with enough space to form hydrates, and the presence of clay makes the pore space smaller in clay-bearing sediments. Although the increase in specific surface area in clay-bearing sediments increases the number of hydrate nucleation sites, and the instantaneous hydrate formation rate is greater than that of the pure quartz sand system when CH_4 is first injected into the reactor, the smaller pore space makes the pore channels easily to be blocked. The subsequent formation of hydrate in clay-bearing sediments is affected by the mass transfer resistance, and thus the hydrate formation rate is slower than that of the pure quartz sand system. As displayed in Fig. 4(b), the hydrate saturation in bentonite-bearing sediments is lower than that in quartz sand and illite-bearing sediments at the end of hydrate formation. That is, part of the water combines with bentonite and changes into bound water which cannot form hydrates. This is because some of the water combines with bentonite and prevents it from forming hydrates. The free water content is unaffected by the presence of illite, in contrast to bentonite-bearing sediments, which merely enhance the specific surface area to speed up the initial hydrate formation rate. Higher hydrate saturation is the result of more complete water-gas contact in illite-bearing sediments as opposed to quartz sand sediments.

The P-wave velocity and amplitude growth rates during hydrate formation are seen to be the fastest in sediments containing bentonite, second in quartz sands, and slowest in sediments containing illite, as illustrated in Fig. 4(c). The results demonstrate that a small amount of water distributes in the larger surface area of bentonite-containing sediments so that the hydrate formation process is rapidly complete, bentonite-hydrate-quartz sand quickly completes cementation due to the smaller pores caused by the swelling of bentonite, while free water does not affect by the illite-containing sediments in which the hydrate is first formed on the surface of the illite, and then gradually cement quartz sand resulting in a slower rise of the P-wave velocity and amplitude. In the end, the magnitude of P-wave velocity and amplitude in different sediments after hydrate formation is finished are arranged in order of hydrate saturation. The speculation in Fig. 4(c) is further supported by the relationship between P-wave velocity and hydrate saturation. Because hydrate mostly forms on the surface of

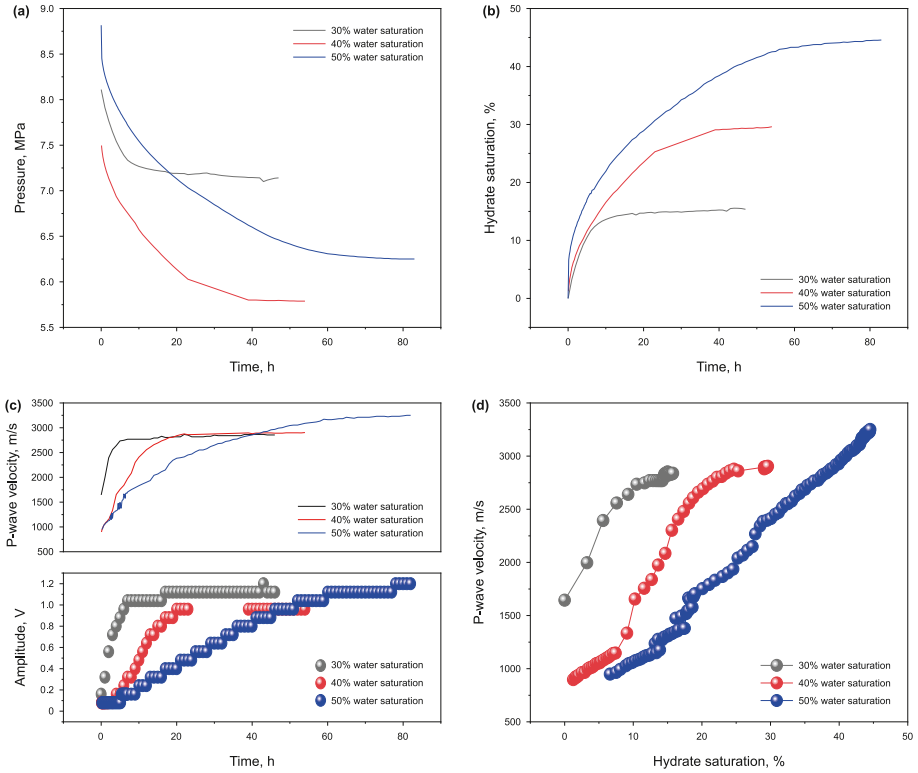

Fig. 3. Variation of **(a)** pressure; **(b)** hydrate saturation; **(c)** P-wave velocity and amplitude with time and **(d)** P-wave velocity with hydrate saturation in different water saturation with 10% bentonite content sediments.

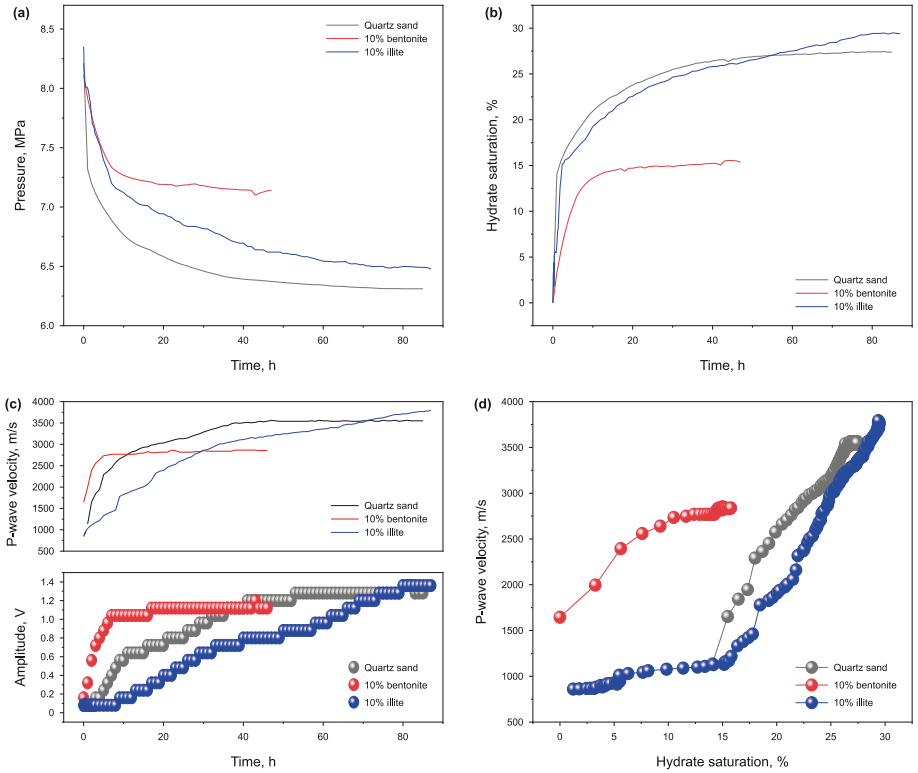

Fig. 4. Variation of **(a)** pressure; **(b)** hydrate saturation; **(c)** P-wave velocity and amplitude with time and **(d)** P-wave velocity with hydrate saturation in different sediments with 30% water saturation.

illite in the pore space, the increase in P-wave velocity with hydrate growth is not substantial for hydrate saturations below 15% (volume). A fast increase in the P-wave velocity occurs once hydrate saturation in illite-bearing sediments surpasses 15% (volume) due to the progressive cementation of illite-hydrate-quartz sand, as shown in Fig. 4(d).

3.2. CH_4 hydrate decomposition

The excess free CH_4 gas was released and the pressure was adjusted to about 0.5 MPa above the equilibrium pressure of CH_4 hydrate once the hydrate formation process was finished. However, the decrease in P-wave velocity and amplitude during the excess free CH_4 gas release might be caused by the hydrate decomposition at the ultrasonic probe, which results in poor contact between the probe and sediment. Similar phenomena have also been reported in the literature (Li et al., 2011). This is the main reason for the inconsistency in P-wave velocity and amplitude before hydrate depressurization mining and after hydrate formation is finished. In this work, all hydrate mining experiments are conducted at 2 MPa and 275.15 K.

3.2.1. Effect of bentonite content

The variation of P-wave velocity and amplitude with time during hydrate mining in sediments with different bentonite content is shown in Fig. 5. It can be seen that the value of V_P decreases by 370 m/s (from 3551 to 3181 m/s) and amplitude decreases by 0.32 V (from 1.28 to 0.96 V) for sediments with 0% (mass) bentonite content within 8 min. Compared to sediments containing bentonite, this is considerably different. The value of V_P decreases by 896 m/s (from 3099 to 2203 m/s) and amplitude decreases by 0.72 V (from 0.96 to 0.24 V) for sediments with 5% (mass) bentonite content within 11 min, while the value of V_P decreases by 545 m/s (from 2726 to 2181 m/s) and amplitude decreases by 0.64 V (from 0.96 to 0.32 V) for sediments with 10% (mass) bentonite content within 9 min, and the value of V_P decreases by 66 m/s (from 1336 to 1270 m/s) and amplitude decreases by 0.08 V (from 0.16 to 0.08 V) for 15% (mass) bentonite content sediments within 7 min. These results, independent of the bentonite content and hydrate saturation, provide strong evidence for the weak cementation between hydrate and sediment in bentonite-bearing sediments. What's more, it is important to note that the P-wave velocity and amplitude in bentonite-bearing sediments strata decline steeply, within about 30 min of the depressurization. On the one hand, the weak cementation of the hydrate with the bentonite-bearing sediments makes the cementation disappear rapidly when the hydrate begins to decompose. On the other hand, the hydrate may be distributed as smaller particles in the bentonite-bearing sediments, which results in a faster hydrate decomposition rate. In addition, despite the various amounts of bentonite and hydrate saturation in the sediments, the overall trend of P-wave velocity and amplitude decreasing during hydrate decomposition is identical, and the main difference lies in the initial stage of hydrate decomposition. It can be found that the higher the initial hydrate saturation is, the more hydrate decomposes in the initial stage after depressurization, resulting in a greater decrease in P-wave velocity and amplitude.

3.2.2. Effect of water saturation

As Fig. 6(a) and (b) illustrate, the P-wave velocity and amplitude show a vertical downward trend in the initial stage after hydrate depressurization. The value of V_P decreases by 856 m/s (from 2727 to 1871 m/s) and amplitude decreases by 0.72 V (from 0.96 to 0.24 V) for 30% (volume) water saturation bentonite-bearing hydrate deposits within 21 min, while the value of V_P decreases by 1027 m/s (from 3037 to 2010 m/s) and amplitude decreases by 0.4 V (from 0.64 to 0.24 V) for 40% (volume) water saturation bentonite-bearing hydrate within 18 min, and the value of V_P decreases by 1239 m/s (from 2963 to 1724 m/s) and amplitude decreases by 0.8 V (from 0.88 to 0.08 V) for 50% (volume) water saturation bentonite-bearing hydrate deposits within 17 min. The results demonstrate that the cementation between hydrate and sediments rapidly disappears in bentonite-bearing sediments when hydrate begins to decompose, and the higher hydrate saturation caused by the higher water saturation, the more the P-wave velocity and amplitude decreases, caused by the more hydrate decomposes in the sediments. As shown in Fig. 6(a), the decreasing trend of P-wave velocity slows down following approximately 50 min after depressurization. That is, in sediments with varying initial hydrate saturations, the rapid hydrate decomposition stage terminates. Subsequently, as the hydrate slowly decomposes, the P-wave velocity decreases slowly. Combined with Fig. 6(b), the amplitude is almost minimized within 50 min after depressurization. This indicates that the cementation of the hydrate with the sediments has completely disappeared and the remaining hydrate fills the pores of the sediment.

The trends of P-wave velocity and amplitude in Fig. 6 illustrate that the presence of bentonite leads to weak cementation between hydrate and quartz sand so that the hydrate is the first to decompose at the surface of the quartz sand, and the cementation disappears rapidly, which makes the mechanical strength of the sediments weak instantly. Therefore, the mining of hydrates in bentonite-bearing sediments is highly susceptible to geohazards, regardless of the hydrate saturation investigated in this study.

3.2.3. Effect of sediments

In order to make hydrate mining safer and more efficient, it is necessary to know the hydrate decomposition characteristics and characterization of acoustic properties in different sediments. As

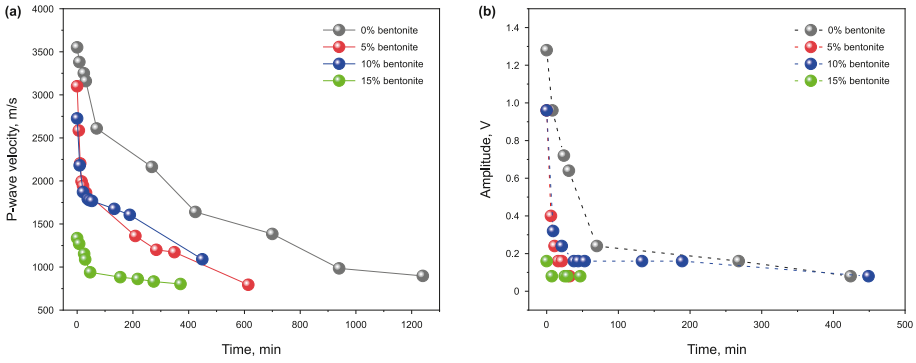

Fig. 5. Variation of **(a)** P-wave velocity and **(b)** amplitude with time during hydrate decomposition in different bentonite containing sediments.

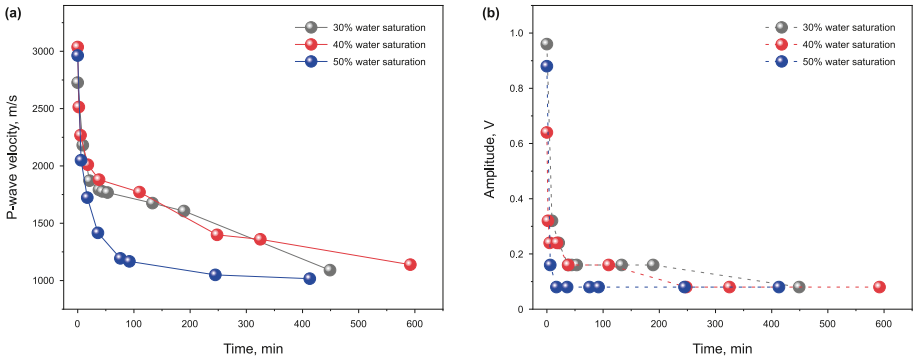

Fig. 6. Variation of **(a)** P-wave velocity and **(b)** amplitude with time during hydrate decomposition in different water saturation with 10% bentonite-bearing sediments.

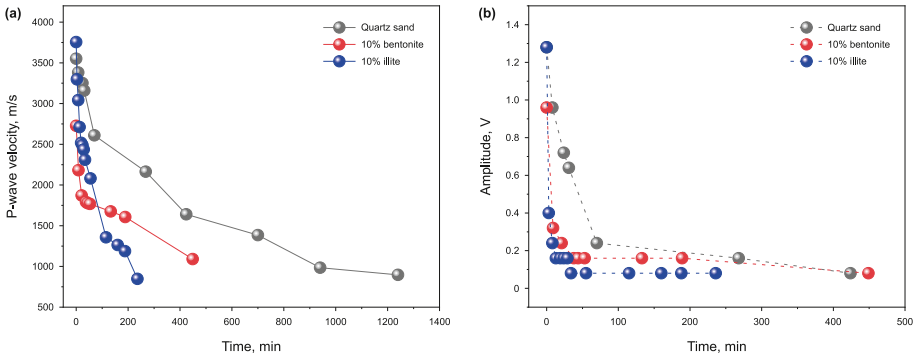

Fig. 7. Variation of **(a)** P-wave velocity and **(b)** amplitude with time during hydrate decomposition in different sediments with 30% water saturation.

can be seen from Fig. 4, hydrate saturation and acoustic properties at the end of hydrate formation are similar for illite-bearing sediments and quartz sand sediments, and the illite-bearing sediments have a greater impact on hydrate partitioning than quartz sand sediments. Although the presence of illite in sediments does not affect the amount of free water involved in hydrate formation, their decomposition characteristics differ significantly. Fig. 7(a) and (b) display that the value of P-wave velocity decreases by 170 m/s (from 3551 to 3381 m/s) and amplitude decreases by 0.32 V (from 1.28 to 0.96 V) for quartz sand within 8 min, while the value of P-wave velocity decreases by 546 m/s (from 2727 to 2181 m/s) and amplitude decreases by 0.64 V (from 0.96 to 0.32 V) for 10% (mass) bentonite containing sediments within 9 min, and the P-wave velocity decreases by 714 m/s (from 3756 to 3042 m/s) and amplitude decreases by 0.88 V (from 1.28 to 0.4 V) for 10% illite containing sediments within 8 min. The results illustrate the presence of clays in the sediments causes the hydrate to be weakly cemented to the sediments, and the cementation rapidly disappears after the depressurization starts, regardless of the type of clay and the degree of hydrate saturation. In addition, the capillary effect generated by the fine-grained clay filling the pores increases the hydrate phase equilibrium pressure, and the hydrate decomposition rate in the clay-bearing sediments is significantly larger than that in the quartz sand sediments. The P-wave velocity and amplitude of hydrate decomposition in clay-bearing sediments change with time, indicating that the risk of geologic hazards increases with hydrate mining in clay-bearing sediments, particularly in the early stage of the process. More importantly, the geologic hazard risks increase with increasing hydrate saturation in the clay-bearing reservoir.

The schematic diagram of hydrate formation and decomposition

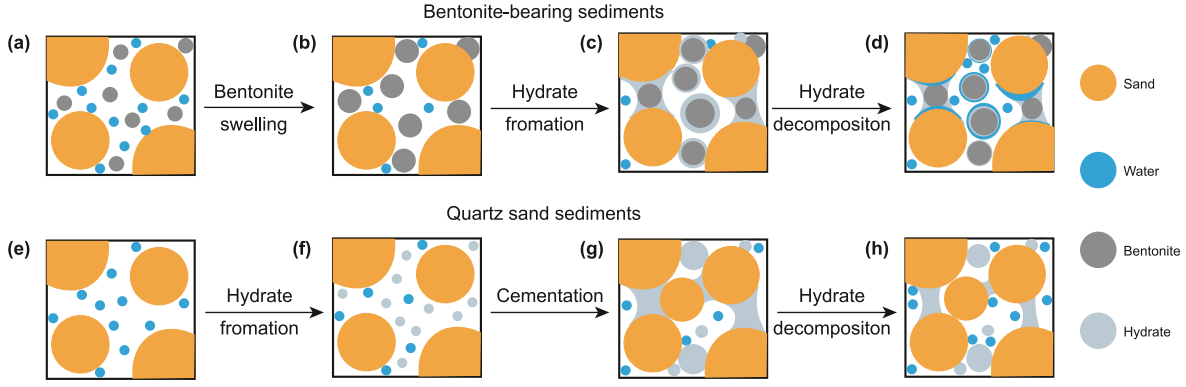

Fig. 8. Schematic diagram of hydrate formation and decomposition in quartz sand and bentonite-bearing sediments.

in quartz sand and clay-bearing sediments (bentonite as an example) is shown in Fig. 8. From the above experimental results, it can be seen that P-wave velocity and amplitude of both hydrate formation and decomposition in bentonite-bearing sediments change rapidly. The reasons for the rapid change in P-wave velocity and amplitude are well explained in Fig. 8, where the bentonite particles absorb water and swell (Fig. 8(a)–(b)), then the hydrate first forms on the surface of bentonite particles and quickly cement with the quartz sand in the smaller pore space (Fig. 8(b)–(c)), and the hydrate first decomposes at the surface contact of the quartz sand (Fig. 8(c)–(d)) is the main reason for the rapid decrease of P-wave velocity and amplitude during hydrate depressurization mining. Unlike bentonite-bearing sediments, hydrates first form in quartz sand pores and gradually aggregate (Fig. 8(e)–(f)). Hydrates begin to cement the quartz sand when the saturation reaches a certain level (Fig. 8(f)–(g)), at this time, the P-wave velocity and amplitude increase rapidly. However, during hydrate depressurization mining, the hydrates preferentially decompose in the pore space (Fig. 8(g)–(h)), gradually becoming smaller and thinner until the cementation of the hydrate with quartz sand disappears. As a result, the P-wave velocity and amplitude decrease more slowly.

4. Conclusions

In this work, in order to better understand the state of hydrate in clay-bearing sediments and to make hydrate mining safer and more efficient, the characteristics of P-wave velocity and amplitude were studied in different bentonite contents sediments, different water saturations with 10% (mass) bentonite containing sediments, and different sediments during hydrate formation and decomposition. The conclusions can be drawn as follows:

(1) During hydrate formation, P-wave velocity and amplitude have similar trends. As the amount of bentonite in the sediment increases, the attenuation of the acoustic signal reduces. The increase in bentonite content accelerates the mutual cementation of hydrate and sediment leading to a faster increase in P-wave velocity and amplitude, and higher bentonite content (10%) at the same hydrate saturation has a faster P-wave velocity. However, too much bentonite reduces the hydrate saturation by affecting the free water content and weakens the cementation between hydrate and sediment. The hydrate first forms on the surface of the bentonite/quartz sand or suspended in its pores as the water saturation increases. As the hydrate saturation rises, they are gradually cemented to one another. Thus, the P-wave velocity is greater at low hydrate saturation when water saturation is low. A comparison of different sediment types shows that neither illite nor quartz sand absorbs water and swells. When hydrate saturation exceeds 15%, sediment and hydrate start to cement one another, and P-wave velocity increases as hydrate saturation increases. It is worth noting that hydrate saturation is approximately positively and linearly correlated with P-wave velocity under different conditions in this work.

(2) During hydrate depressurization, P-wave velocity decreases gradually with hydrate decomposition. The hydrate in clay-bearing sediments shows a faster decomposition rate, and the P-wave velocity decreases faster. In particular, the amplitude drops linearly at the instant of depressurization which can be attributed to the weak cementation of hydrates to sediments in clay-bearing sediments. As a result, hydrate mining in clay-bearing sediments is especially prone to strata destabilization, which can lead to geohazards.

CRediT authorship contribution statement

Yi-Jian Zhu: Writing – original draft, Methodology, Investigation, Conceptualization. **Xiao-Mei Yang:** Investigation. **Xing Huang:** Investigation. **Hao Li:** Investigation. **Xiao-Hui Wang:** Validation. **Yi-Fei Sun:** Investigation. **Peng Xiao:** Formal analysis. **Chang-Yu Sun:** Writing – review & editing, Supervision, Funding acquisition, Conceptualization. **Guang-Jin Chen:** Supervision.

Declaration of competing interest

The authors declare that they have no known competing financial interests or personal relationships that could have appeared to influence the work reported in this paper.

Acknowledgements

This work was financially supported by the National Key Research and Development Program of China (No. 2021YFC2800902), the Basic Research Program of Qinghai Province (2023-ZJ-703), and the National Natural Science Foundation of China (Nos. 22178379, 22127812).

References

Bu, Q.T., Hu, G.W., Liu, C.L., et al., 2019. Acoustic characteristics and micro-distribution prediction during hydrate dissociation in sediments from the South China Sea. J. Nat. Gas Sci. Eng. 65, 135–144. https://doi.org/10.1016/j.jngse.2019.02.010.

Chen, G.J., Guo, T.M., 1998. A new approach to gas hydrate modelling. Chem. Eng. J. 71 (2), 145–151. https://doi.org/10.1016/S1385-8947(98)00126-0.

Chen, J., Wang, Y.H., Lang, X.M., et al., 2015. Energy-efficient methods for production methane from natural gas hydrates. J. Energy Chem. 24 (5), 552–558. https://doi.org/10.1016/j.jechem.2015.08.014.

Ding, J.P., Cheng, Y.F., Deng, F.C., et al., 2020. Experimental study on dynamic acoustic characteristics of natural gas hydrate sediments at different depths. Int. J. Hydrogen Energy. 45 (51), 26877–26889. https://doi.org/10.1016/j.ijhydene.2020.06.295.

Guo, K., Fan, S.S., Wang, Y.H., et al., 2020. Physical and chemical characteristics analysis of hydrate samples from northern South China sea. J. Nat. Gas Sci. Eng. 81, 103476. https://doi.org/10.1016/j.jngse.2020.103476.

Kadoura, A., Nair, A.K.N., Sun, S.Y., 2016. Molecular dynamics simulations of carbon dioxide, methane, and their mixture in montmorillonite clay hydrates. J. Phys. Chem. C. 120 (23), 12517–12529. https://doi.org/10.1021/acs.jpcc.6b02748.

Kim, H.S., Cho, G.C., Kwon, T.H., 2013. Effect of CO_2 hydrate formation on seismic wave velocities of fine-grained sediments. G-cubed. 14 (6), 1787–1799. https://doi.org/10.1002/ggge.20102.

Li, F.G., Sun, C.Y., Zhang, Q., et al., 2011. Laboratory measurements of the effects of methane/tetrahydrofuran concentration and grain size on the P-Wave velocity of hydrate-bearing sand. Energy Fuel. 25 (5), 2076–2082. https://doi.org/10.1021/ef101665v.

Li, Y.H., Liu, W.G., Zhu, Y.M., et al., 2016. Mechanical behaviors of permafrost-associated methane hydrate-bearing sediments under different mining methods. Appl. Energy. 162, 1627–1632. https://doi.org/10.1016/j.apenergy.2015.04.065.

Li, Y.H., Luo, T.T., Sun, X., et al., 2019. Strength Behaviors of remolded hydrate-bearing marine sediments in different drilling depths of the South China Sea. Energies 12 (2), 1–14. https://doi.org/10.3390/en12020253.

Liu, Z., Kim, J., Lei, L., et al., 2019. Tetrahydrofuran hydrate in clayey sediments—laboratory formation, morphology, and wave characterization. J. Geophys. Res. Solid Earth. 124 (4), 3307–3319. https://doi.org/10.1029/2018jb017156.

Lv, T., Li, X., Chen, Z., et al., 2019. Effect of fulvic acid and sodium chloride on the phase equilibrium of methane hydrate in mixed sand–clay sediment. J. Chem. Eng. Data. 64 (2), 632–639. https://doi.org/10.1021/acs.jced.8b00884.

Ning, F.L., Liang, J., Wu, N., et al., 2020. Reservoir characteristics of natural gas hydrates in China. Nat. Gas. Ind. 40, 1–24. https://doi.org/10.3787/j.issn.1000-0976.2020.08.001.

Qian, J., Wang, X.J., Collett, T.S., et al., 2018. Downhole log evidence for the coexistence of structure II gas hydrate and free gas below the bottom simulating reflector in the South China Sea. Mar. Petrol. Geol. 98, 662–674. https://doi.org/10.1016/j.marpetgeo.2018.09.024.

Ren, L.L., Jiang, M., Wang, L.B., et al., 2020a. Gas hydrate exploitation and carbon dioxide sequestration under maintaining the stiffness of hydrate-bearing sediments. Energy 194, 116869. https://doi.org/10.1016/j.energy.2019.116869.

Ren, L.L., Qi, Y.H., Chen, J.L., et al., 2020b. Dependence of acoustic properties on hydrate-bearing sediments with heterogeneous distribution. Appl. Energy 275,

115211. https://doi.org/10.1016/j.apenergy.2020.115211.
Ren, S.R., Liu, Y.J., Liu, Y.X., et al., 2010. Acoustic velocity and electrical resistance of hydrate bearing sediments. J. Petrol. Sci. Eng. 70 (1–2), 52–56. https://doi.org/10.1016/j.petrol.2009.09.001.
Sadeq, D., Alef, K., Iglauer, S., et al., 2018. Compressional wave velocity of hydrate-bearing bentheimer sediments with varying pore fillings. Int. J. Hydrogen Energy. 43 (52), 23193–23200. https://doi.org/10.1016/j.ijhydene.2018.10.169.
Shi, K.J., Wang, Z.F., Jia, Y.X., et al., 2022. Effects of the vertical heterogeneity on the gas production behavior from hydrate reservoirs simulated by the fine sediments from the South China Sea. Energy 255, 124525. https://doi.org/10.1016/j.energy.2022.124525.
Sloan, E.D., 2003. Fundamental principles and applications of natural gas hydrates. Nature 426 (6964), 353–359. https://doi.org/10.1038/nature02135.
Waite, W.F., Santamarina, J.C., Cortes, D.D., et al., 2009. Physical properties of hydrate-bearing sediments. Rev. Geophys. 47 (4), 1–38. https://doi.org/10.1029/2008rg000279.
Wang, R., Liu, T.L., Ning, F.L., et al., 2019a. Effect of hydrophilic silica nanoparticles on hydrate formation: insight from the experimental study. J. Energy Chem. 30, 90–100. https://doi.org/10.1016/j.jechem.2018.02.021.
Wang, J.L., Wu, S.G., Kong, X., et al., 2018. Geophysical characterization of a fine-grained gas hydrate reservoir in the Shenhu area, northern South China Sea: integration of seismic data and downhole logs. Mar. Petrol. Geol. 92, 895–903. https://doi.org/10.1016/j.marpetgeo.2018.03.020.
Wang, L.B., Cui, J.L., Sun, C.Y., et al., 2021. Review on the applications and modifications of the Chen–Guo Model for hydrate formation and dissociation. Energy Fuel. 35 (4), 2936–2964. https://doi.org/10.1021/acs.energyfuels.0c03977.
Wang, X.H., Xu, Q., He, Y.N., et al., 2019b. The acoustic properties of sandy and clayey hydrate-bearing sediments. Energies 12 (10), 1–11. https://doi.org/10.3390/en12101825.
Wu, Z.R., Li, Y.H., Sun, X., et al., 2018. Experimental study on the effect of methane hydrate decomposition on gas phase permeability of clayey sediments. Appl. Energy. 230, 1304–1310. https://doi.org/10.1016/j.apenergy.2018.09.053.
Wu, Z.R., Liu, W.G., Zheng, J.A., et al., 2020. Effect of methane hydrate dissociation and reformation on the permeability of clayey sediments. Appl. Energy. 261, 114479. https://doi.org/10.1016/j.apenergy.2019.114479.
Yan, K.F., Li, X.S., Chen, Z.Y., et al., 2019. Methane hydrate formation and dissociation behaviors in montmorillonite. Chin. J. Chem. Eng. 27 (5), 1212–1218. https://doi.org/10.1016/j.cjche.2018.11.025.
Ye, J.L., Wen, Q.X., Wei, X.W., et al., 2020. Main progress of the second gas hydrate trial production in the South China Sea. Chin. Geol. 47 (3), 557–568. https://doi.org/10.12029/gc20200301.
Yun, T.S., Francisca, F.M., Santamarina, J.C., et al., 2005. Compressional and shear wave velocities in uncemented sediment containing gas hydrate. Geophys. Res. Lett. 32 (10), 1–5. https://doi.org/10.1029/2005gl022607.
Zhang, W., Xu, C.G., Li, X.S., et al., 2023. Microscopic study on the key process and influence of efficient synthesis of natural gas hydrate by in situ Raman analysis of water microstructure in different systems with temperature drop. J. Energy Chem. 82, 317–333. https://doi.org/10.1016/j.jechem.2023.03.029.
Zhang, Y., Zhang, L., Chen, C., et al., 2022. Role of different types of water in bentonite clay on hydrate formation and decomposition. Chin. J. Chem. Eng. 50, 310–316. https://doi.org/10.1016/j.cjche.2022.08.001.
Zhao, D.B., Wan, S.M., 2014. Research progress of clay minerals in sediments of the South China Sea and its application to paleoclimatic reconstruction. Mar. Geol. Quat. Geol. 34 (4), 163–171. https://doi.org/10.3724/SP.J.1140.2014.04163.
Zhu, L.Q., Sun, J., Zhou, X.Q., et al., 2023. Well logging evaluation of fine-grained hydrate-bearing sediment reservoirs: considering the effect of clay content. Petrol. Sci. 20 (2), 879–892. https://doi.org/10.1016/j.petsci.2022.09.018.